Current Biology, Volume *21*

Supplemental Information

Ndc80 Internal Loop Interacts with Dis1/TOG to Ensure Proper Kinetochore-Spindle Attachment in Fission Yeast

Kuo-Shun Hsu and Takashi Toda

Inventory of Supplemental Information

Supplemental Figures (Figures S1-S4)
Supplemental Movies S1-S4 legends (movies available online)
Supplemental Table S1: Fission yeast strains used in this study
Supplemental Table S2: Plasmids used in this study
Supplemental Experimental Procedures
Supplemental References

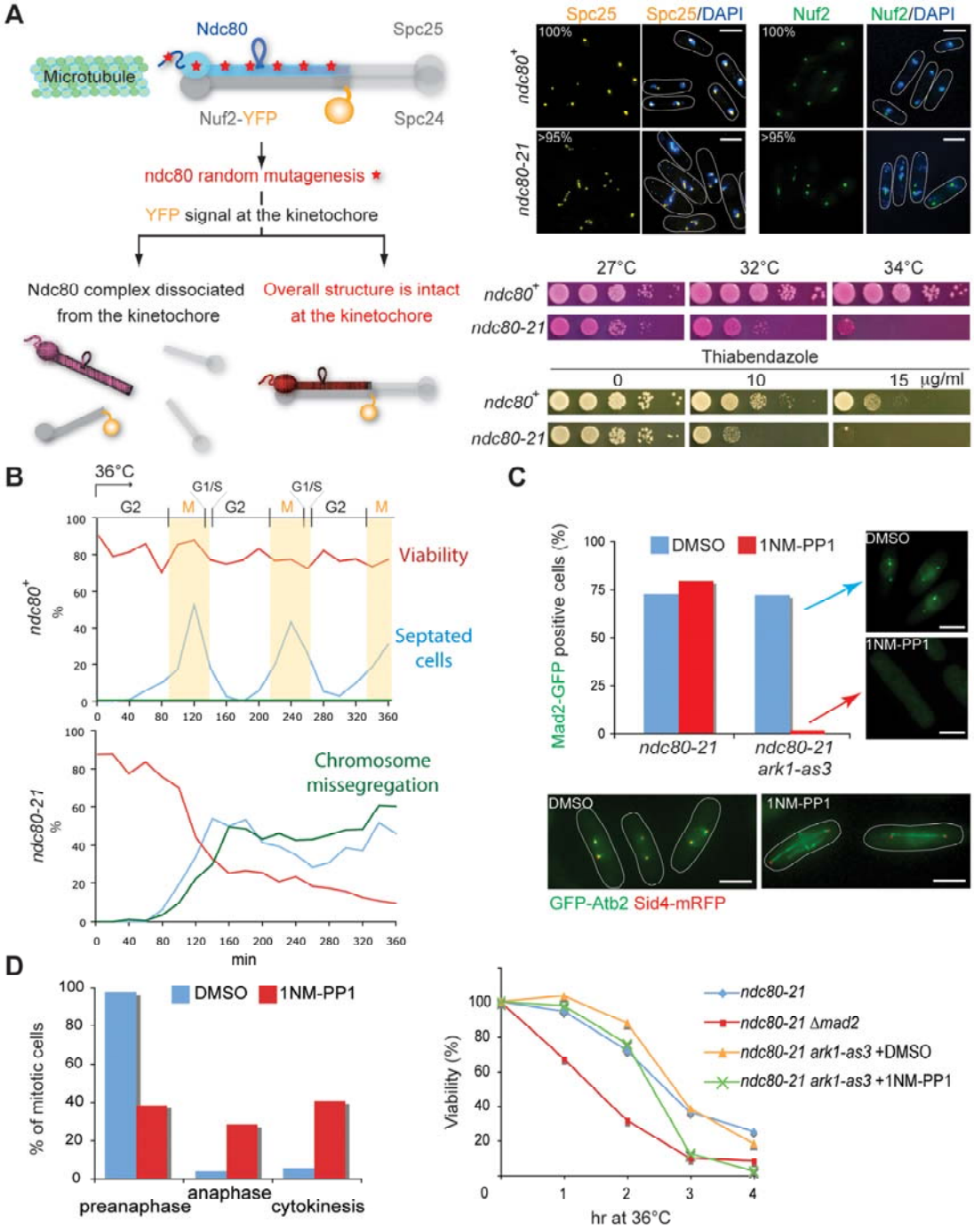

Figure S1 (related to Figure 1): The temperature-sensitive *ndc80-21* mutant retains kinetochore-localizing capability accompanied with activation of the spindle assembly checkpoint

(A) Isolation of the *ndc80-21* mutant. Schematic presentation of *ndc80* mutant isolation is shown on the left. Ndc80 plays multiple roles at the kinetochore, such as overall kinetochore assembly [S1] and spindle assembly checkpoint (SAC) signaling and therefore, if Ndc80 function were completely abolished at the restrictive temperature, such loss-of-function mutants would display pleiotropic

phenotypes, conundrums in delineating specific spindle phenotypes. In order to overcome this foreseen drawback, we devised the screening strategy. We reasoned that kinetochore assembly or SAC function would require localization of the Ndc80 complex to the kinetochore. Given this assumption, we intended to isolate ts *ndc80* mutants that retained kinetochore-localizing activities. In order to assess whether isolated ts mutants retained capability of kinetochore localization, each mutant was tagged with Nuf2-YFP or Spc25-YPF and YFP signals were observed at the restrictive temperature. If the Ndc80 complex fails to be formed, no YFP signals would be detected at the kinetochores (bottom left). However if YFP signals were detected at kinetochores, we assume that activities of complex formation and kinetochore localization are intact in mutants.

Kinetochore localization of the Ndc80 complex in the *ndc80-21* mutant is shown on the top right. Wild type (top 4 panels) or *ndc80-21* mutant cells (lower 4 panels) containing Spc25-YFP (4 panels on the left) or Nuf2-YFP (4 panels on the right) were incubated at 6 h at the restrictive temperature 36˚C. Fluorescent images (orange for Spc25 and green for Nuf2) were shown together with DAPI (blue). Temperature- and thiabendazole-sensitivity is shown on the bottom right. Tenfold serial dilutions of wild type (wt) or *ndc80-21* cells were spotted onto rich agar media (containing the red phloxine B dye, $5X10^4$ cells in the first spot) and incubated at the indicated temperatures for 3 d. The same set of strains were spotted on rich media containing the anti-microtubule drug, thiabendazole (0, 10 or 15 μg/ml) and incubated at 27˚C for 4 d. Scale bars, 5 μm.

(B) Cell viability (wild type; upper, *ndc80-21*; lower) in synchronous culture analysis. Small G2 cells grown at 27°C were collected with centrifugal elutriation and shifted to 36°C at time 0. At each time-point, aliquots of cells were taken and plated on rich YES5 plates. Viability was calculated from the number of viable colonies divided by actual cell number. In addition other aliquots were fixed and stained with DAPI (to monitor chromosome segregation patterns, green) and Calcofluor (a dye staining septa, blue). Light orange columns mark periods in mitosis. n > 200.

(C) SAC silencing by Aurora B inactivation. *ndc80-21* and analogue-sensitive *ndc80-21 ark1-as3* cells [12] containing Mad2-GFP were shifted to 36°C. 1NM-PP1 (5 μM) or DMSO was added to each culture 30 min after temperature shift up. These cultures were left for another 60 min and observed under fluorescence microscope. Mad2-GFP kinetochore dots were no longer retained in the absence of Ark1 function (top, see images on the right). Note that morphologies of anaphase B spindles look normal in *ndc80-21 ark1-as3* cells treated with 1NM-PP1 (bottom right). Scale bars, 5 μm.

(D) Consequence of Aurora B and Mad2 inactivation in *ndc80-21*. Percentages of cells corresponding to preanaphase, anaphase and cytokinetic stages were counted (left, n > 200). In order to measure viability drop, cultures of indicated *ndc80-21* strains were shifted from 27°C to 36°C at time 0 and aliquots were spread on rich plates and incubated at 27°C (right). DMSO or 1NM-PP1 was added 30 min after temperature shift up. Note that *ndc80-21 mad2* double mutants lost viability much faster than *ndc80-21 ark1-as3* cells (in the presence of 1NM-PP1). Therefore residual 30% of mitotic *ndc80-21 ark1-as3* cells in the presence of 1NM-PPI (left) might be ascribable to incomplete inactivation of Ark1-as3 by NM-PP1. Alternatively the requirement of Mad2 and Ark1 for SAC activity might not be identical. In other words, unlike *mad2* deletion, residual SAC activities might be maintained in the absence of Ark1 function.

Supplementary results and discussion derived from Figure S1:

As anaphase spindles in *ndc80-21 ark1-as3* appear normal (Figure S1C), we posit that *ndc80-21* is specifically defective in forming stable prometaphase/metaphase spindles under SAC activation, but this mutant is capable of organizing anaphase B spindles properly once the SAC is silenced. This implies that Ndc80 is not involved in a global organization of mitotic spindle microtubules, but instead it is required exclusively for proper kinetochore microtubule assembly.

Morphological defects of spindle microtubules have not been described in earlier publications that characterized the Mis12 kinetochore component [S2, S3]. As the Mis12 complex tethers the Ndc80 complex to the kinetochore [S4, S5], *mis12* mutants may be deemed to show similar spindle defects to those of *ndc80-21*. However, as shown in Figure S1C (lower) and discussed earlier, *ndc80-21* exhibited nearly normal morphologies of elongated anaphase B spindles once the SAC is silenced. We suspect that this is one of the reasons that defects of pre-anaphase spindle morphologies were never detected or described [S2, S3]. When Mis12 function is disrupted, the SAC is no longer activated, and as a result pre-anaphase mitotic phase is very transient. Accordingly appearance of unstable pre-anaphase spindles would have been simply overlooked, particularly by the usage of fixed still images with conventional immunofluorescence microscopy, on which previous work depended [S2, S3].

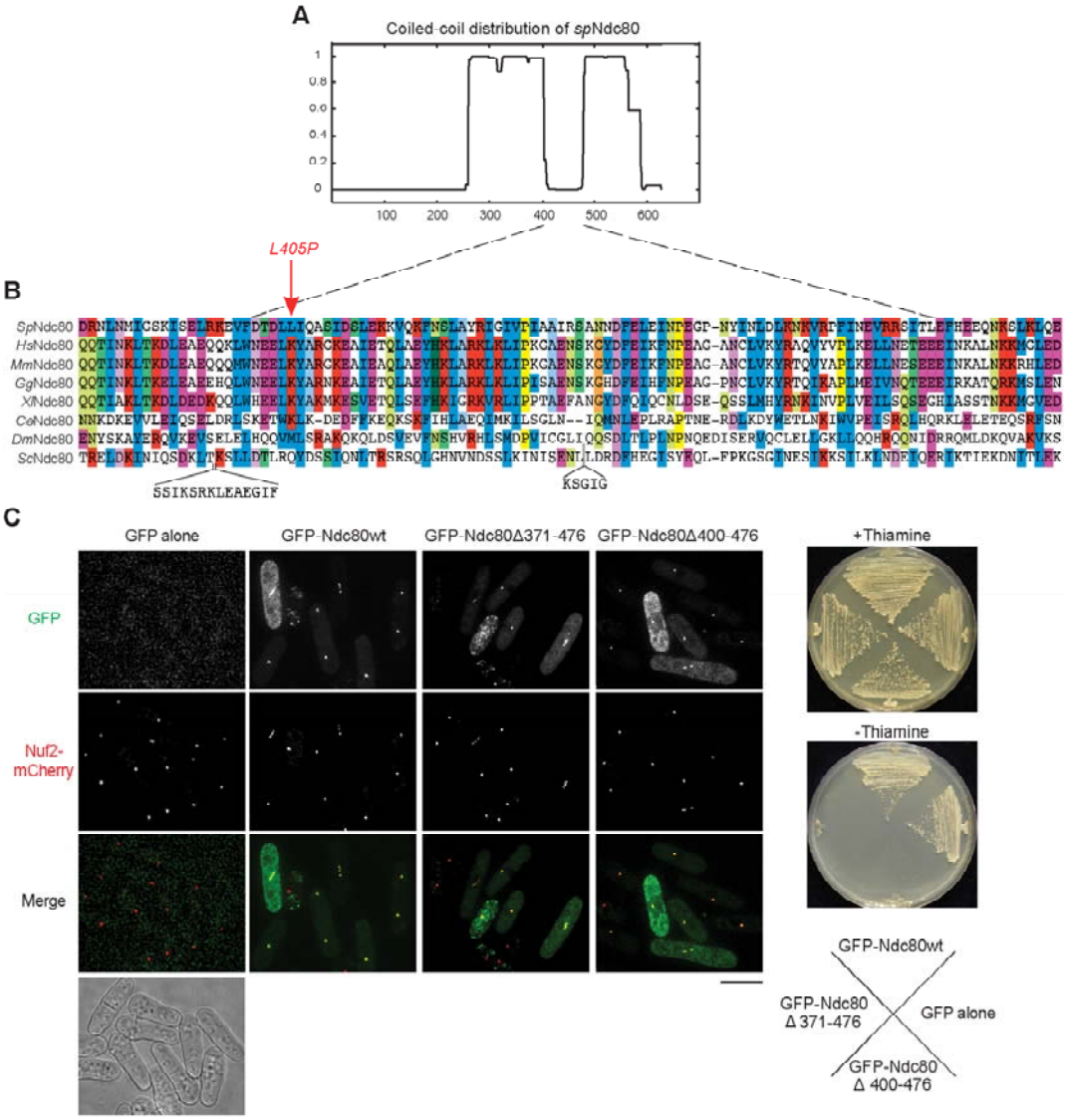

Figure S2 (related to Figure 2): The mutation site of Ndc80-21 in the internal loop and kinetochore localization of loop-less Ndc80.

(A) Coiled coil scores profile of the Ndc80 protein.

(B) Amino acid residues corresponding to the internal loop of Ndc80 from different species are aligned. L405, which is mutated to P in *ndc80-21*, is marked with an arrow.

(C) Kinetochore localization of loop-less Ndc80. Cells containing plasmids expressing wild type Ndc80 or two types of loop-less Ndc80 (Ndc80Δ400-476 and Ndc80Δ371-476) under the thiamine-repressible *nmtP41* promoter were streaked on minimal plates in the presence (top right, repressed) or absence of thiamine (middle, derepressed) and incubated at 30°C for 3d. The same strains (containing Nuf2-mCherry) were cultured in liquid minimal media (in the absence of thiamine) at 30°C for 16 h and fluorescence images were taken. Note that dotted GFP signals colocalized with Nuf2-mCherry. Some cells showed non-specific uniform background GFP signals, as Ndc80 was overproduced from the *nmt* promoter. DIC image was shown on the bottom left in order to clarify cell morphologies. Scale bar, 5 μm.

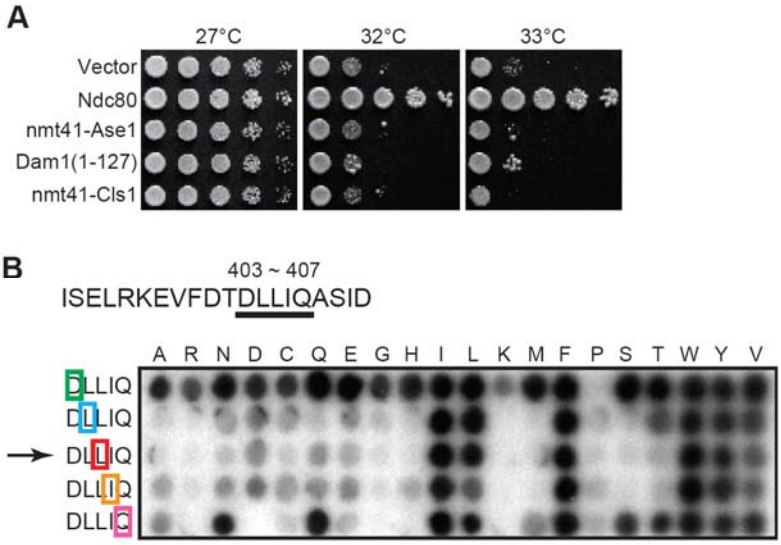

Figure S3 (related to Figure 3): Dis1 binds directly to the Ndc80 internal loop

(A) Multicopy plasmids containing indicated genes were transformed into an *ndc80-21* strain and spot test was performed at the indicated temperatures. Dis1 and Alp14 are homologues of the Dis1/TOG family [S6, S7]. However, unlike Dis1, Alp14's spindle localization requires Alp7/TACC [S7, S8]. Peg1/Cls1 is a homologue of human CLASP [S9, S10]. Ase1 is a homologue of human PRC1 [S11, S12]. Mal3 is a homologue of human EB1 [S13, S14] (see Figure 3A). Multicopy plasmids producing full-length or a truncated activated version of Dam1 (Dam1-1-127) [33] also failed to suppress *ndc80-21*.

(B) Analysis of residues in the loop essential for interaction with Dis1. 20 amino acid-length peptides (shown on the top) each containing a single mutation in one of the DLLIQ region (underlined on the top and boxed in the lower left side) were spotted on a membrane, which was then incubated with GST-Dis1, followed by immunoblotting with anti-GST antibody. Each peptide has one residue replaced with one of the 20 amino acids. Data shown in Figure 3E is marked with an arrow.

Supplementary results and discussion derived from Figure S3:

Despite several previous publications, morphologies of unstable spindle microtubules in *dis1* mutants have not been described [24, S15, S16]. This is, however, not discrepancy with our findings. We notice that in those previous studies, microtubules were observed either at the non-restrictive temperatures or with conventional immunofluorescence microscopy using anti-tubulin antibodies. Without the combined usage of the strict restrictive temperature (20°C) and time-lapse live imaging of microtubules (GFP-Atb2), unstable pre-anaphase microtubules would not have been noticed nor would they be properly interpreted. In fact these unstable microtubules (two blobs without inter-SPB microtubules) were reported previously as anaphase B spindles in which the central part was depolymerized.

Four ts *nuf2* mutants (*nuf2-1, -2, -3* and *-4*) were previously isolated and characterized [S17]. Although the authors acknowledged activation of the SAC in some alleles (*nuf2-2* and *-3*) and the appearance of long anaphase B spindles, unstable pre-anaphase spindle phenotypes were not described [S17]. We suppose that the usage of immunofluorescence microscopy with anti-tubulin

antibodies without synchronization might have contributed to the differences from our interpretations. Alternatively it is formally possible that in these *nuf2* mutants, pre-anaphase spindle microtubules are not destabilized.

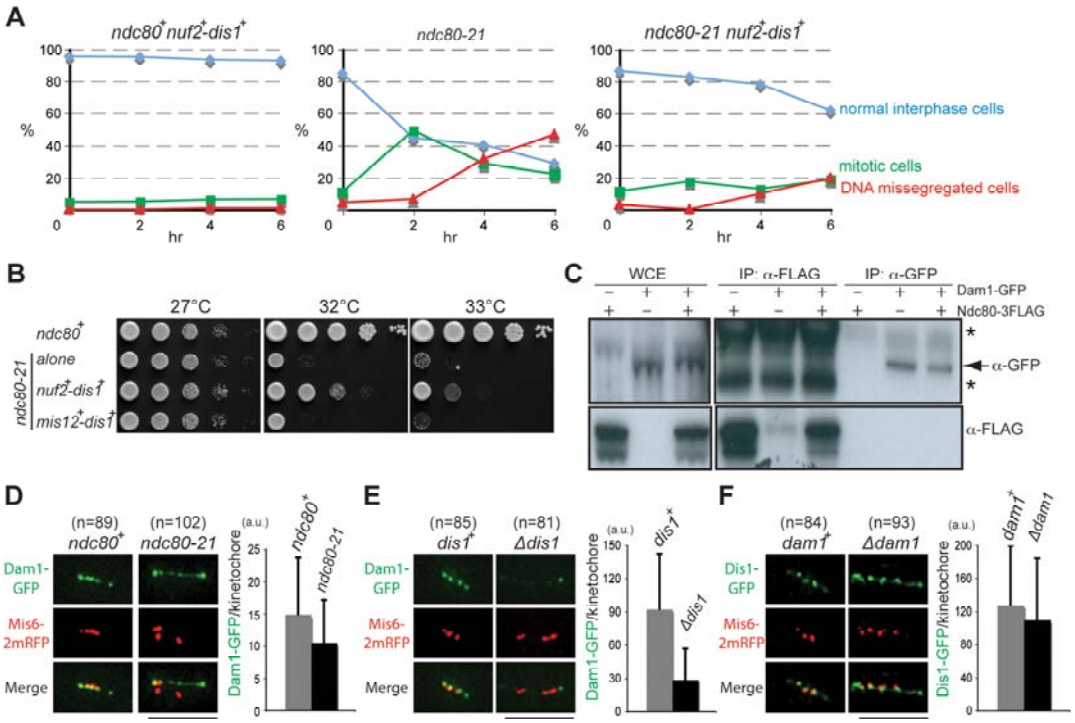

Figure S4 (related to Figure 4): Rescue of *ndc80-21* by Dis1 tethering to Nuf2 and potential involvement of the Dam1 complex

(A) Suppression of ts *ndc80-21* by Dis1 fused with Nuf2. Indicated strains were grown in liquid media at 32°C. At 0, 2, 4 and 6 h time points, cells were fixed and stained with DAPI and Calcofluor, by which percentages of mitotic cells (a readout of SAC activation) and interphase cells showing chromosome missegregation (an indicator for kinetochore malfunction) were calculated.

(B) Fusion of Dis1 with Mis12 did not rescue *ndc80-21.*

An *ndc80-21* strain containing the Mis12-Dis1 fusion protein was constructed (Supplemental Experimental Procedures) and spot tests were performed at indicated temperatures. Pictures were taken after 3 d incubation.

(C) Ndc80 and Dam1 do not co-precipitate. Cell extracts were prepared from three metaphase arrested *cut9-665* strains that contained Dam1-GFP only, Ndc80-3FLAG only or Dam1-GFP and Ndc80-3FLAG together, followed by reciprocal immunoprecipitation using anti-FLAG or anti-GFP antibody as a primary antibody. No coimmunoprecipitation was seen in either case. Asterisks were IgG bands. WCE; whole cell extract [1.67 mg extracts were used for immunoprecipitation and 50 μg were run as WCE].

(D-F) Dependency of kinetochore localization. Kinetochore localization of Dam1-GFP signal intensities were reduced to ~70% in the *ndc80-21* mutant incubated at 36°C for 2 h (D), whilst they dropped down to ~30% in the *dis1* deletion incubated at 20°C for 4 h (E). In contrast intensities of Dis1-GFP signals were in large not significantly altered in the *dam1* deletion (>90%, F) incubated at 20°C for 6 h. Error bars represent the standard deviation. Scale bars, 5 μm.

Supplementary results and discussion derived from Figure S4:

Recently it is shown that in budding yeast Ndc80 interacts with the Dam1 complex [S18,S19]. Binding between these two complexes appears indirect, as it

requires microtubules. More relevantly to our work, Tanaka and colleagues have found that it is the internal loop of Ndc80 that is critical for this interaction (T. U. Tanaka, personal communication). In fission yeast, unlike budding yeast, the Dam1 complex is not essential, but nonetheless this complex plays an important role in proper spindle-kinetochore attachment [33, 34, S20-S24]. Our results shown in Supplemental figures indicated the following three points. First Dam1 localization to mitotic kinetochores is lessened in either *ndc80-21* or *dis1* deletion mutants (Figure S4D and S4E). Second Dis1 kinetochore signals, on the other hand, do not alter significantly in the *dam1* deletion (Figure S4F). Third unlike Dis1, Dam1 do not bind Ndc80 (Figure S4C). These results may point toward a possibility that the Dam1 complex acts downstream of Dis1 with regards to kinetochore localization. However it is also possible that, as Dam1 localization to the kinetochore requires intact spindle microtubules [33], apparent delocalization of Dam1 from kinetochores simply reflects unstable spindle microtubules in *ndc80-21* or *dis1* mutants. Consequently we could not draw solid conclusions at the moment on the involvement of the Dam1 complex in the Ndc80 loop/Dis1-dependent attachment of the kinetochore to spindle microtubules. It should be also important to note that in fission yeast Dam1 localization to the kinetochore is dependent on another component Dad1 [32, 33], whose kinetochore localization in turn requires Mis6 (a homolog of budding yeast Ctf3 and human CENP-I), but not Mis12, which is essential for kinetochore localization of the Ndc80 complex [S4, S5]. Thus it appears that the mechanism of Dam1 kinetochore localization is not identical at most and rather could be different between budding yeast and fission yeast.

In D*rosophila*, Ndc80 and XMAP215/TOG directly or indirectly interact [S25]. Genome-wide RNAi analysis of the whole human genes shows that knockdown of human TOG/CKAP5 results in severe mitotic defects that are similar, if not identical, to those found in knockdown of Ndc80 complex components [S26]. Also it is known that knockdown of Ndc80 complex components render kinetochore microtubules extremely unstable [S27, S28]. Further analysis is necessary to address evolutionary conservation of roles for Ndc80 and Dis1/TOG in microtubule dynamics and spindle-kinetochore attachment.

Supplemental Movies Legends (movies available online)

Movie S1: Mitotic progression of wild type (corresponding to Figure 1A, top three rows)

Fluorescent proteins used are Mis6-2mRFP (kinetochore) and GFP-Atb2 (microtubule). Anaphase B starts within 10 min (see Figure 1A for time scale).

Movie S2: Mitotic arrest of *ndc80-21* (corresponding to Figure 1A, bottom three rows)

Fluorescent proteins used are Mis6-2mRFP (kinetochore) and GFP-Atb2 (microtubule). Note a prolonged mitotic stage (> 50 min) with unstable spindle microtubules.

Movie S3: *cen2*-GFP movement during wild type mitosis (corresponding to Figure 1B, upper)

Centromere on chromosome II are visualized with GFP (*cen2*-GFP) and SPBs are marked with Sad1-dsRed. *cen2*-GFP splits into two at around 8 min (see Figure 1B for time scale).

Movie S4: *cen2*-GFP movement during *ndc80-21* mitosis (corresponding to Figure 1B, lower)

Centromere on chromosome II are visualized with GFP (*cen2*-GFP) and SPBs are marked with Sad1-dsRed. Note that a pair of *cen2*-GFP signals locates in close proximity to one of the SPBs (top).

Table S1: Fission yeast strains used in this study

Strains	Genotypes	Figures used
KSH002	*h⁻ nuf2⁺-YFP-ura4⁺ leu1 ura4*	S1A
KSH059	*h⁻ ndc80-21-kan^r nuf2⁺-YFP-ura4⁺ leu1 ura4*	S1A
KSH107	*h⁻ spc25⁺-YFP-nat^r leu1 ura4*	S1A
KSH139	*h⁻ ndc80-21-kan^r spc25⁺-YFP-nat^r leu1 ura4*	S1A
KSH153	*h⁻ ndc80-21-kan^r kan^r-GFP-atb2⁺ mis6⁺-2mRFP-hph^r cut12⁺-CFP- nat^r leu1 ura4*	1A, 1B, S1B, 2B 2D,
KSH163	*h⁻ kan^r-GFP-atb2⁺ mis6⁺-2mRFP-hph^r cut12⁺-CFP-nat^r leu1 ura4*	1A, 1B, S1B, 2C, 2E-G, 3H
KSH206	*h⁻ cen2(D107)-kan$_r$-ura4₊-lacOp his7⁺-lacI-GFP-ura4⁺ sad1⁺-dsRed-leu2⁺ leu1 ura4*	1C
KSH221	*h⁻ ndc80-21-kan^r cen2(D107)-kan$_r$-ura4₊-lacOp his7⁺-lacI-GFP-ura4⁺ sad1⁺-dsRed-LEU2 leu1 ura4*	1C
KSH224	*h⁻ mad2⁺-GFP-leu2⁺ mis6⁺-2mRFP-hph^r cut12⁺-CFP- nat^r leu1*	1D
KSH228	*h⁻ ndc80-21-kan^r mad2⁺-GFP-LEU2 mis6⁺-2mRFP-hph^r cut12⁺-CFP- nat^r leu1 ura4*	1D
KSH397	*h⁺ ndc80-21-kan^r ark1-as3-hph^r mad2⁺-GFP-leu2⁺ cut12⁺-CFP- nat^r (leu1)*	S1C, S1D
KSH398	*h⁻ ndc80-21-kan^r mad2⁺-GFP-leu2⁺ cut12⁺-CFP-nat^r (leu1)*	S1C
KSH550	*h⁻ ndc80-21-kan^r ark1-as3-hph^r kan^r-GFP-atb2⁺ sid4⁺-mRFP- nat^r leu1*	S1C, S1D
KSH060	*h⁻ ndc80-21-kan^r leu1 ura4*	S1D, 3A, 4A-C, S4A, S4B
KSH291	*h⁺ ndc80-21-kan^r mad2::ura4⁺ leu1 ura4 his2*	S1D
KSH003	*h⁻ nuf2⁺-mCherry-ura4⁺ leu1 ura4*	S2C
KSH499	*h⁻ cut9-665 dis1⁺-8Myc-leu2⁺ (ura4)*	3B
KSH545	*h⁻ cut9-665 dis1⁺-8Myc-leu2⁺ ndc80⁺-3Flag-kan^r (leu1)*	3B

KSH546	*h⁻ cut9-665 ndc80⁺-3Flag-kan^r leu1*	3B, S4C
KSH510	*h⁺ ndc80⁺-3Flag-kan^r leu1 ura4 his2*	3C
KSH466	*h⁻ kan^r-nmt41-GFP-dis1⁺ mis6⁺-2mRFP-hph^r cut12⁺-CFP- nat^r leu1 ura4 his7*	3F, 3G
KSH467	*h⁻ ndc80-21-kan^r kan^r-nmt41-GFP-dis1⁺ mis6⁺-2mRFP-hph^r cut12⁺-CFP- nat^r leu1 ura4 his2 (his7)*	3F
KSH576	*h⁻ dis1::ura4⁺ kan^r-GFP-atb2⁺ mis6⁺-2mRFP-hph^r cut12⁺-CFP- nat^r leu1 ura4*	3H
513	*h⁻ leu1 ura4*	4A, S4B
KSH555	*h⁺ ndc80-21-kan^r nuf2⁺-dis1(18-882)-nat^r leu1 ura4 his2*	4A-C, S4A, S4B
KSH556	*h⁻ ndc80-21-kan^r nuf2⁺-dis1(18-518)-nat^r leu1 ura4*	4A
KSH557	*h⁻ ndc80-21-kan^r nuf2⁺-dis1(518-882)-nat^r leu1 ura4*	4A
KSH552	*h⁻ nuf2⁺-dis1(18-882)-nat^r leu1 ura4*	4B, 4C, S4A
KSH637	*h⁻ ndc80-21-kan^r mis12⁺-dis1(18-882)-nat^r leu1 ura4*	S4B
KSH592	*h⁻ cut9-665 dam1⁺-GFP-kan^r leu1*	S4C
KSH595	*h⁻ cut9-665 ndc80⁺-3Flag-kan^r dam1⁺-GFP-kan^r leu1*	S4C
KSH582	*h⁻ ndc80-21-kan^r dam1⁺-GFP-kan^r mis6⁺-2mRFP-hph^r cut12⁺-CFP- nat^r leu1 ura4 his7*	S4D
KSH583	*h⁻ dam1⁺-GFP-kan^r mis6⁺-2mRFP-hph^r cut12⁺-CFP- nat^r leu1 ura4 his7*	S4D, S4E
KSH589	*h⁻ dis1::ura4⁺ dam1⁺-GFP-kan^r mis6⁺-2mRFP-hph^r cut12⁺-CFP- nat^r leu1 ura4 his7*	S4E
KSH597	*h⁻ dis1⁺-GFP-ura4⁺ mis6⁺-2mRFP-hph^r cut12⁺-CFP- nat^r leu1 ura4*	S4F
KSH599	*h⁻ dam1::kan^r dis1⁺-GFP-ura4⁺ mis6⁺-2mRFP-hph^r cut12⁺-CFP- nat^r leu1 ura4 ade6*	S4F

Table S2: Plasmids used in this study

Name	Gene	Origin*
pAL-SK-Alp14	*alp14*+	our stock
pREP1-Ase1	*ase1*$^{+}$	our stock
pREP41-Ase1	*ase1*$^{+}$	our stock
pSB123	*cls1*$^{+}$	F. Chang
pUR19-Dam1(full length)	*dam1*$^{+}$	J. Millar
pUR19-Dam1(1-127)	*dam1*	J. Millar
pSK-Dis1	*dis1*$^{+}$	our stock
pKZ17	*mal3*$^{+}$	our stock
pREP1-Ndc80	*ndc80*$^{+}$	This study
pREP1-Ndc80-T307A	*ndc80*	This study
pREP1-Ndc80-E379G	*ndc80*	This study
pREP1-Ndc80-L405P	*ndc80*	This study
pREP1-Ndc80-T307A/E379G	*ndc80*	This study
pREP1-Ndc80-E379G/L405P	*ndc80*	This study
pREP1-Ndc80Δ371-476	*ndc80*	This study
pREP1-Ndc80Δ400-476	*ndc80*	This study
pREP1-Ndc80Δ2-94	*ndc80*	This study
pREP41-GFP-Ndc80	*ndc80*	This study
pREP41-GFP-Ndc80Δ371-476	*ndc80*	This study
pREP41-GFP-Ndc80Δ400-476	*ndc80*	This study

*Plasmids were constructed for this study unless otherwise specified.

Supplemental Experimental Procedures

Isolation of ts *ndc80* mutants that retain kinetochore-localizing activities

The kanamycin-resistance marker gene cassette (*kan^r*) was inserted in the 3' flanking region of the *ndc80$^+$* gene (*ndc80$^+$-kan^r*). The *ndc80$^+$-kan^r* fragment purified from this strain was amplified with error-prone PCR using Vent DNA polymerase (New England Biolabs Ltd.) supplemented with 10X deoxyguanosine triphosphate (dGTP). Pools of mutagenized PCR fragments were ethanol precipitated and transformed into a wild-type strain (513, Supplemental Table S1). Approximately 3,000 transformants were screened for temperature sensitivity at 36^{o}C and 15 ts mutants were isolated. These mutants were crossed with a strain containing *nuf2$^+$-YPF-ura4$^+$* or *spc25$^+$-YPF-nat^r* (Nourseothricin). Individual kanamycin-resistant Ura$^+$ (for Nuf2-YFP) or kanamycin- and nourseothricin-resistant segregants (for Spc25-YFP) were tested for temperature-sensitivity and localization of Nuf2-YFP or Spc25-YFP at kinetochores. 7 ts mutants including *ndc80-21* clearly retained kinetochore-localizing activities of Nuf2 or Spc25 (>80% intensity compared to wild type) at the restrictive temperature (see Figure S1A).

The mutation sites in *ndc80-21*

Nucleotide sequencing of genomic DNA isolated from the *ndc80-21* mutant showed four point mutations within the ORF of the *ndc80-21* gene, *T889C*, *A1011G*, *A1228G* and *T1306C* (the first adenine for the initiator methionine is denoted as 1). These changes predict one silent mutation and the following three missense mutations, T307A, E379G and L405P (Figure 2A).

Construction of multicopy plasmids carrying wild type or mutant *ndc80* gene

The whole ORF of the *ndc80$^+$* gene was PCR-amplified and cloned into

*Nde*I/*Bam*HI sites of pREP1, which carries the thiamine repressible *nmt1* promoter [S29], designated pREP-Ndc80 (verified by nucleotide sequencing). Various *ndc80* mutants (T307A, E379G, L405P, T307A/E379G and E379G/L405P, used in Figure 2B) were then constructed using QuikChange kit (Stratagene Co. U. S. A.) with pREP-Ndc80 as a template. Plasmids producing truncated Ndc80 mutants (∆loop and ∆N tail, used in Figures 2C-2G and 3G) were constructed from PCR-amplified *ndc80* fragments. Ndc80∆loop lacks the internal residues between 400-476 or 371-476, whilst Ndc80∆N tail lacks 2-94 amino acid residues. All the mutations were verified by nucleotide sequencing. As it takes more than 12 h at 30^{o}C for genes under control of the *nmt1* promoter to be overexpressed [S29], observations started and cell extracts were prepared after 14 h induction (Figure 2C and 2E-2G).

Microscopy

Images were taken using an Olympus IX70 wide-field inverted epifluorescence microscope with an Olympus PlanApo 100×, NA 1.4, oil immersion objective. DeltaVision image acquisition software (softWoRx 3.3.0; Applied Precision) equipped with Coolsnap HQ (Roper Scientific) was used. The sections of images at each time point were compressed into a two-dimensional (2D) projection using the DeltaVision maximum intensity algorithm. Deconvolution was applied before the 2D projection. Kymograph pictures derived from 2D-projected time-lapse images were constructed using softWoRx 3.3.0. Images were taken as 14–18 sections along the *z* axis at 0.25- to 0.3-mm intervals; they were then deconvolved and merged into a single projection. For some experiments, an AxioplanII microscope (Zeiss Lts.) with Volocity software (Improvision Co.) was

also used. Captured images were processed with Adobe Photoshop CS3 (version 10.0).

Fluorescence signal intensity quantification

Images were merged into a single projection using maximum intensity algorithm in Deltavision-SoftWoRx (Olympus and Applied Precision Ltd.). Fluorescence signals were then quantified using maximum intensity, after subtracting background signals in the vicinity of the fluorescent spot (Figures 3F and S4D-F).

Preparation of synchronous cultures using HU

In order to accumulate mitotic cells, HU-induced S phase arrest and release was used (Figures 3C, 3G, S1C and S1D). Cultures were treated with 12 mM hydroxyurea (HU) at 25^{o}C for 4 h, filtered and incubated HU-free media at 30^{o}C (Figure 3C and 3G). For inactivation of Ark1 (Figure S1C and S1D), 5 μM 1NM-PP1 was added to the culture after 30 min incubation at 36^{o}C. Upon further 60 min incubation at 36^{o}C, cells were observed under fluorescent microscope.

Immunoprecipitation using M-phase arrested *cut9-665*

Immunoprecipitation was performed using standard procedures as briefly described below (Figures 3B and S4C). *cut9-665* mutants were grown at 26°C overnight and then shifted to 36°C for 3.5 h. Proteins were extracted in IP buffer [50 mM Tris-HCl pH 7.4, 1 mM EDTA pH 8.0, 500 mM NaCl, 0.05% NP-40, 0.1% Triton X-100, 10% glycerol, 1 mM dithiothreitol, 15 mM p-nitrophenyl phosphate, 1 mM PMSF, and protease inhibitor cocktail (Sigma)] by breaking the cells at 4°C with glass beads (setting 5.5, 25 s, 2x) in a FastPrep FP120 apparatus (Savant. Co, MN, USA). The protein extracts were collected after 15 min of centrifugation at 13,000 x g at 4°C. The coimmunoprecipitations were performed by adding protein extracts to protein A dynabeads (Invitrogen Ltd. CA, USA) bound with

anti-FLAG antibody (M2, Sigma-Aldrich UK). For immunoblotting, anti-FLAG and anti-Myc (MMS-150R, Covance Inc. CA, USA) antibodies were used at 1:1000 and 1: 2000, respectively.

GST pull down assay

GST-Dis1 (18-882) fusion protein was produced in *E. coli* and purified with Glutathione-Sepharose beads as recommended by the manufacturer (Invitrogen, Carlsbad, CA, U. S. A.). Gel filtration was further applied to increase the protein purity (used in Figures 3C-3E and S3B). Yeast cell extracts were prepared from a strain containing Ndc80-3FLAG upon HU arrest-release. Glutathione-Sepharose beads bound with GST alone or GST-Dis1 were incubated with the cell extracts at 4°C for 2 h. After washing 4 times with IP buffer, the bound proteins were eluted with reduced glutathione, separated by SDS-PAGE and immunoblotted with anti-FLAG antibody (M2, Sigma-Aldrich UK, Figure 3C).

Binding assay between Dis1 and Ndc80-loop mutants

Rabbit polyclonal anti-Ndc80 antibodies were prepared by Eurogenetec Co. (Belgium). Peptides H_2N-CRETASEEKNAFDAE-$CONH_2$ were used to raise sera, which were affinity-purified before usage (used in Figure 3G). *nmt41-GFP-dis1*$^+$ cells carrying episomal pREP1-Ndc80 or pREP1-Ndc80Δ371-476 were grown in the absence of thiamine for 12 h at 30°C, followed by HU arrest for 4 h at 25°C and release at 36°C for 1.5 h. Cell extracts were prepared from these cultures and immunoprecipitation was performed with anti-Ndc80 antibodies, followed by immunoblotting with anti-Ndc80 (1:100) and anti-GFP (1814 460, Roche Diagnostics, Indianapolis, IN) antibodies (1:1000).

Peptide array assay

Procedures described previously [S4] were basically followed with slight

modifications (Figures 3D, 3E and S3B). Peptides were synthesized and spotted onto a cellulose membrane. The membrane was activated by treatment with 50% ethanol + 10% glacial acetic acid for 1 h and then washed with IP buffer. 1 μg/ml of GST-Dis1 or GST alone was then added to the solution. After overnight incubation at 4°C, the membrane was blocked with 3% skim milk in the same buffer, followed by incubation with anti-GST antibody (27457701V, GE Healthcare Life Science) for 2 h at room temperature. After further washes, spots with bound GST-Dis1 were detected using bovine anti–goat IgG-HRP–conjugated secondary antibody (sc-2378, Santa Cruz Biotechnology) and visualized by chemiluminescence.

Construction of strains containing *nuf2-dis1* and *mis12-dis1* fusion genes

DNA fragments encoding Nuf2-Dis1 (amino acid 18-882), Nuf2-Dis1N (amino acid 18-518) and Nuf2-Dis1C (amino acid 518-882), flanked by the C-terminal nourseothricin (nat^r)-resistant marker [S30], were amplified by using two-step PCR. These fragments were transformed into a *nuf2*$^+$-*YFP-ura4*$^+$ strain (KSH002, Table S1) and integrants were selected on 5'FOA (5-fluoro-orotic acid)- and nourseothricin (nat^r)-containing plates. Correct integrations were checked by colony PCR or nucleotide sequencing (used in Figure 4A). Basically the same procedures were followed to construct the *mis12*$^+$-*dis1*$^+$ fusion gene except that in this case, *mis12*$^+$-*dis1*$^+$ fragments followed by the *nat*^{r} maker were directly amplified with PCR and transformed into an *ndc80-21* strain (Figure S4B).

Supplemental References

S1. McCleland, M.L., Gardner, R.D., Kallio, M.J., Daum, J.R., Gorbsky, G.J., Burke, D.J., and Stukenberg, P.T. (2003). The highly conserved Ndc80 complex is required for kinetochore assembly, chromosome congression, and spindle checkpoint activity. Genes Dev. *17*, 101-114.

S2. Saitoh, S., Ishii, K., Kobayashi, Y., and Takahashi, K. (2005). Spindle checkpoint signaling requires the Mis6 kinetochore subcomplex, which interacts with Mad2 and mitotic spindles. Mol. Biol. Cell *16*, 3666-3677.

S3. Goshima, G., Saitoh, S., and Yanagida, M. (1999). Proper metaphase spindle length is determined by centromere proteins Mis12 and Mis6 required for faithful chromosome segregation. Genes Dev. *13*, 1664-1677.

S4. Maskell, D.P., Hu, X.W., and Singleton, M.R. (2010). Molecular architecture and assembly of the yeast kinetochore MIND complex. J. Cell Biol. *190*, 823-834.

S5. Petrovic, A., Pasqualato, S., Dube, P., Krenn, V., Santaguida, S., Cittaro, D., Monzani, S., Massimiliano, L., Keller, J., Tarricone, A., et al. (2010). The MIS12 complex is a protein interaction hub for outer kinetochore assembly. J. Cell Biol. *190*, 835-852.

S6. Garcia, M.A., Vardy, L., Koonrugsa, N., and Toda, T. (2001). Fission yeast ch-TOG/XMAP215 homologue Alp14 connects mitotic spindles with the kinetochore and is a component of the Mad2-dependent spindle checkpoint. EMBO J. *20*, 3389-3401.

S7. Sato, M., Vardy, L., Garcia, M.A., Koonrugsa, N., and Toda, T. (2004). Interdependency of fission yeast Alp14/TOG and coiled coil protein Alp7 in microtubule localization and bipolar spindle formation. Mol. Biol. Cell *15*,

1609-1622.

S8. Sato, M., and Toda, T. (2007). Alp7/TACC is a crucial target in Ran-GTPase-dependent spindle formation in fission yeast. Nature *447*, 334-337.

S9. Grallert, A., Beuter, C., Craven, R.A., Bagley, S., Wilks, D., Fleig, U., and Hagan, I.M. (2006). *S. pombe* CLASP needs dynein, not EB1 or CLIP170, to induce microtubule instability and slows polymerization rates at cell tips in a dynein-dependent manner. Genes Dev. *20*, 2421-2436.

S10. Bratman, S.V., and Chang, F. (2007). Stabilization of overlapping microtubules by fission yeast CLASP. Dev. Cell *13*, 812-827.

S11. Yamashita, A., Sato, M., Fujita, A., Yamamoto, M., and Toda, T. (2005). The roles of fission yeast Ase1 in mitotic cell division, meiotic nuclear oscillation and cytokinesis checkpoint signaling. Mol. Biol. Cell *16*, 1378-1395.

S12. Loiodice, I., Staub, J., Gangi-Setty, T., Nguyen, N.P., Paoletti, A., and Tran, P.T. (2005). Ase1p organizes anti-parallel microtubule arrays during interphase and mitosis in fission yeast. Mol. Biol. Cell *16*, 1756-1768.

S13. Beinhauer, J.D., Hagan, I.M., Hegemann, J.H., and Fleig, U. (1997). Mal3, the fission yeast homologue of the human APC-interacting protein EB-1 is required for microtubule integrity and the maintenance of cell form. J. Cell Biol. *139*, 717-728.

S14. Asakawa, K., Toya, M., Sato, M., Kanai, M., Kume, M., Goshima, T., Garcia, M.A., Hirata, D., and Toda, T. (2005). Mal3, the fission yeast EB1 homolog, cooperates with Bub1 spindle checkpoint to prevent monopolar attachment. EMBO Rep. *6*, 1194-1120.

S15. Nabeshima, K., Kurooka, H., Takeuchi, M., Kinoshita, K., Nakaseko, Y.,

and Yanagida, M. (1995). p93^{dis1}, which is required for sister chromatid separation, is a novel microtubule and spindle pole body-associating protein phosphorylated at the Cdc2 target sites. Genes Dev. *9*, 1572-1585.

S16. Zheng, L., Schwartz, C., Magidson, V., Khodjakov, A., and Oliferenko, S. (2007). The spindle pole bodies facilitate nuclear envelope division during closed mitosis in fission yeast. PLoS Biol. *5*, e170.

S17. Nabetani, A., Koujin, T., Tsutsumi, C., Haraguchi, T., and Hiraoka, Y. (2001). A conserved protein, Nuf2, is implicated in connecting the centromere to the spindle during chromosome segregation: a link between the kinetochore function and the spindle checkpoint. Chromosoma *110*, 322-334.

S18. Lampert, F., Hornung, P., and Westermann, S. (2010). The Dam1 complex confers microtubule plus end-tracking activity to the Ndc80 kinetochore complex. J. Cell Biol. *189*, 641-649.

S19. Tien, J.F., Umbreit, N.T., Gestaut, D.R., Franck, A.D., Cooper, J., Wordeman, L., Gonen, T., Asbury, C.L., and Davis, T.N. (2010). Cooperation of the Dam1 and Ndc80 kinetochore complexes enhances microtubule coupling and is regulated by aurora B. J. Cell Biol. *189*, 713-723.

S20. Franco, A., Meadows, J.C., and Millar, J.B. (2007). The Dam1/DASH complex is required for the retrieval of unclustered kinetochores in fission yeast. J. Cell Sci. *120*, 3345-3351.

S21. Griffiths, K., Masuda, H., Dhut, S., and Toda, T. (2008). Fission yeast *dam1-A8* mutant is resistant to and rescued by an anti-microtubule agent. Biochem. Biophys. Res. Commun. *368*, 670–676.

S22. Saitoh, S., Kobayashi, Y., Ogiyama, Y., and Takahashi, K. (2008). Dual

regulation of Mad2 localization on kinetochores by Bub1 and Dam1/DASH that ensure proper spindle interaction. Mol. Biol. Cell *19*, 3885-3897.

S23. Kobayashi, Y., Saitoh, S., Ogiyama, Y., Soejima, S., and Takahashi, K. (2007). The fission yeast DASH complex is essential for satisfying the spindle assembly checkpoint induced by defects in the inner-kinetochore proteins. Genes Cells *12*, 311-328.

S24. Gao, Q., Courtheoux, T., Gachet, Y., Tournier, S., and He, X. (2010). A non-ring-like form of the Dam1 complex modulates microtubule dynamics in fission yeast. Proc. Natl. Acad. Sci. USA *107*, 13330-13335.

S25. Bucciarelli, E., Pellacani, C., Naim, V., Palena, A., Gatti, M., and Somma, M.P. (2009). *Drosophila* Dgt6 interacts with Ndc80, Msps/XMAP215, and γ-tubulin to promote kinetochore-driven MT formation. Curr. Biol. *19*, 1839-1845.

S26. Hutchins, J.R., Toyoda, Y., Hegemann, B., Poser, I., Heriche, J.K., Sykora, M.M., Augsburg, M., Hudecz, O., Buschhorn, B.A., Bulkescher, J., et al. (2010). Systematic analysis of human protein complexes identifies chromosome segregation proteins. Science *328*, 593-599.

S27. DeLuca, J.G., Moree, B., Hickey, J.M., Kilmartin, J.V., and Salmon, E.D. (2002). hNuf2 inhibition blocks stable kinetochore-microtubule attachment and induces mitotic cell death in HeLa cells. J. Cell Biol. *159*, 549-555.

S28. McCleland, M.L., Kallio, M.J., Barrett-Wilt, G.A., Kestner, C.A., Shabanowitz, J., Hunt, D.F., Gorbsky, G.J., and Stukenberg, P.T. (2004). The vertebrate Ndc80 complex contains Spc24 and Spc25 homologs, which are required to establish and maintain kinetochore-microtubule attachment. Curr. Biol., 131-137.

S29. Maundrell, K. (1990). *nmt1* of fission yeast. J. Biol. Chem. *265*,

10857-10864.

S30. Sato, M., Dhut, S., and Toda, T. (2005). New drug-resistant cassettes for gene disruption and epitope tagging in *Schizosaccharomyces pombe*. Yeast *22*, 583-591.